

Simultaneous Ultrasound and MRI System for Breast Biopsy: Compatibility Assessment and Demonstration in a Dual Modality Phantom

Annie M. Tang, Daniel F. Kacher, Edmund Y. Lam*, *Senior Member, IEEE*, Kelvin K. Wong, Ferenc A. Jolesz, and Edward S. Yang, *Fellow, IEEE*

Abstract—Simultaneous capturing of ultrasound (US) and magnetic resonance (MR) images allows fusion of information obtained from both modalities. We propose an MR-compatible US system where MR images are acquired in a known orientation with respect to the US imaging plane and concurrent real-time imaging can be achieved. Compatibility of the two imaging devices is a major issue in the physical setup. Tests were performed to quantify the radio frequency (RF) noise introduced in MR and US images, with the US system used in conjunction with MRI scanner of different field strengths (0.5 T and 3 T). Furthermore, simultaneous imaging was performed on a dual modality breast phantom in the 0.5 T open bore and 3 T close bore MRI systems to aid needle-guided breast biopsy. Fiducial based passive tracking and electromagnetic based active tracking were used in 3 T and 0.5 T, respectively, to establish the location and orientation of the US probe inside the magnet bore. Our results indicate that simultaneous US and MR imaging are feasible with properly-designed shielding, resulting in negligible broadband noise and minimal periodic RF noise in both modalities. US can be used for real time display of the needle trajectory, while MRI can be used to confirm needle placement.

Index Terms—Breast biopsy, magnetic resonance imaging (MRI), multimodality imaging, tracking, ultrasound (US).

I. INTRODUCTION

MULTIMODALITY imaging has great benefit for diagnosis and therapy if the strengths of each modality can be fully appreciated, while ameliorating the weakness of any individual one. For example, recent research efforts in the development of concurrent hybrid imaging systems such as X-ray/magnetic resonance imaging (MRI) systems (XMR) [1]–[3] for interventions gathered much interest, and the clinical applications

Manuscript received July 30, 2007; revised October 11, 2007. This work was supported in part by the Research Grant Council of the HKSAR under Project HKU7139/06E and in part by the University Research Committee of the University of Hong Kong under Project 10207440. The work of D. Kacher was supported by the National Institutes of Health under Grant 1U41RR019703-01A2. *Asterisk indicates corresponding author.*

A. M. Tang and E. S. Yang are with Department of Electrical and Electronic Engineering, The University of Hong Kong, Hong Kong.

*E. Y. Lam is with Department of Electrical and Electronic Engineering, The University of Hong Kong, Pokfulam Road, Hong Kong (e-mail: elam@eee.hku.hk).

D. F. Kacher and F. A. Jolesz are with Department of Radiology, Brigham and Women's Hospital, Harvard Medical School, Boston, MA 02115 USA.

K. K. Wong is with Department of Radiology, The Methodist Hospital Research Institute, Houston, TX 77030 USA.

Color versions of one or more of the figures in this paper are available online at <http://ieeexplore.ieee.org>.

Digital Object Identifier 10.1109/TMI.2007.911000

of positron emission tomography (PET)/computer tomography (CT) systems (PET/CT) [4]–[6] and PET/MR systems [7], [8] in clinical oncology have been a great success.

Sequential MRI and ultrasound (US) imaging at different stations with subsequent data fusion has had impact on diagnostic and interventional procedures. For example, carotid artery dispensability and vessel wall function has been measured with duplex Doppler/B-mode US cine images registered with 3-D MRI volumes [9]–[12]. Another example application is in image-guided therapy where navigation is employed. Postprocessing techniques have also been reported for registering preoperative MRI volumes with intraoperative US images for brain deformation estimations and corrections in neurosurgery to improve targeting accuracy [13]–[16]. The tissue contrast of preprocedure MRI has been used to enhance targeting in US-guided breast biopsy and thermal ablation for liver metastases [17], [18]. Nevertheless, the time and inconvenience in imaging a patient in multiple hospital areas or interventional suites, as well as the technical challenges in image fusion due to changes in body orientations and physiological status between scans, has led to the desire for a truly hybrid MRI and US (MR/US) imaging modality.

Hybrid MR/US imaging has several important advantages over other hybrid imaging systems. First, both MRI and US offer three 3-D nonionizing noninvasive imaging capabilities. MRI has exquisite soft tissue contrast with multiplanar imaging characteristics, but with a relatively long imaging time. On the other hand, US is low cost, highly portable, has high temporal resolution available to perform real time Doppler flow measurement, but with a poor tissue discrimination ability. Therefore, the two imaging modalities can potentially compensate the exact weakness of the other when integrated. Second, other hybrid techniques such as XMR require large size fixtures to be built to accommodate the X-ray system in MRI, making the X-ray system suitable only for dedicated use with a single MRI system [1], [3]. Yet the US system is relatively simple in design and highly portable and therefore minimum modifications are required for it to become MRI-compatible while keeping its portability. Thus, the MR-compatible US system can be used more effectively, such as by relocating to serve multiple MRI sites.

In breast biopsy, stereotactic (X-ray guided) and freehand US guidance are increasingly applied in core needle guidance, replacing open surgical biopsy for assessment of breast lesions [19], [20]. Compared to stereotactic guidance, freehand US does not have ionizing radiation but has a high frame rate that

allow one to follow the trajectory of needle during the biopsy process. However, freehand US has a limited field of view and lacks 3-D multiplanar positional information. The position of the target lesions and needle tip may easily be misinterpreted, especially if the numerous lesions are closely positioned, or the biopsy needle and the US probe imaging plane has an in plane error after insertion of the needle [21]. In recent years, MRI has also been adopted for needle guidance for breast biopsies, since breast MR imaging is known to have high sensitivity in lesion detection and allows 3-D visualizations of breast structures with a large field of view [22]–[25]. Typically, an open breast coil is used with the patient in prone position and the breast immobilized by two compression plates with a stereotactic grid. The grid is used to locate the suspected mass and indicate the insertion point of the needle. Targeting accuracy is limited by the grid holes size and error due to needle deflection. Limited patient access inside the bore requires the patient be iteratively removed for needle positioning and moved back in for reimaging to confirm needle position. Thus, the process is time consuming. Recent research on real-time US to guide needle or therapeutic probe placement using preprocedure MRI has shown a significant increase in targeting accuracy when compared with single modality needle guidance [17], [18]. Nevertheless, it still faces great challenges in multimodal image registrations due to nonsimultaneous imaging, and suffer long imaging time for moving a patient to and from different imaging sites.

In this paper, we propose an MR-compatible US system where concurrent real-time imaging can be achieved. We present methods to assess the compatibility when integrating the two imaging systems and investigate the source of image artifacts that appear in both modalities, extending our earlier work [26], [27]. Furthermore, simultaneous imaging was demonstrated on a dual modality breast phantom in 0.5 T open bore and 3 T close bore MRI system to aid needle-guided breast biopsy. To our knowledge, it is one of the first detailed reports on compatibility test and practical setup of concurrent MR/US imaging for breast biopsy. Earlier, MR/US imaging has been reported for real time motion compensation of a motion phantom in MRI for cine cardiac imaging and *in vivo* imaging [28]–[30]. However, in our study, one important concern is the physical setup and mitigation of the cross-talk that exists as a result of interference between the two imaging devices. We performed compatibility tests to establish and verify a method of shielding the US probe inside the magnet bore. The effectiveness of the shielding method was tested by capturing image noise pattern in US and MRI with the MRI RF transmitter power turned off. For simultaneous MR/US scan plane localization for biopsy needle insertion, an electromagnetic-based active tracking system was employed in 0.5 T open bore and fiducial based passive tracking was done in 3 T close bore MRI system to track the position and orientation of the US probe inside the magnet bore. MR images were acquired in a known orientation with respect to US imaging plane.

The results show that concurrent MR/US imaging is feasible with properly-designed shielding, resulting in negligible broadband noise and minimal periodic RF noise in both modalities. With this dual-modality imaging system, real time US can be

used for real time display of the needle trajectory, while MRI can be used to confirm needle placement.

II. MATERIAL AND METHODS

Our work is divided into two parts. In the first part, we quantify the RF noise introduced into the MR and US images when the US probe and beam-former box were placed in the magnet room. In the second part, we demonstrate the simultaneous acquisition of MR and US images for needle biopsy guidance in a breast phantom with an electromagnetic tracker or fiducial markers attached to the US probe head.

A. Experimental Setup

The experiments were carried out in 0.5 T open bore and 3 T close bore MRI systems (Signa SP and Signa Excite HD, GE Medical Systems, Milwaukee, WI). A commercially available PC based portable US system (model T3000, Terason, Burlington, MA) with a 128 element linear array transducer (6–10 MHz) for breast imaging was employed. The US transducer was connected to a beam-forming engine box of size 17 cm × 14 cm × 2 cm inside the magnet room, while the box was connected to a laptop computer outside the room via a waveguide through a 25 m firewire cable. The engine box was entirely powered by the firewire cable, so that no external ac power is needed.

Suitable shielding was mandatory on the US system to limit the RF interference introduced into the MR images. Aluminum foil was contiguously applied to the entire length of US probe cable, engine box, and the firewire cable. The aluminum foil layers and the braid shielding of the firewire cable were grounded to the shielding of the magnetic room, at the penetration panel. The window of the transducers was wrapped with a single layer of aluminum foil, thin enough to allow the penetration of the US signals while minimizing interference in the MR images. To mitigate the effects of magnetic attraction, the steel enclosure around the engine box was replaced with an aluminum enclosure. In our setup with a 0.5 T open bore MRI system, the firewire cable was routed through the 56-cm vertical gap used for surgery within the magnet, to emulate a clinical situation in the intraoperative open bore scanner. For our setup with a 3 T close bore MRI system, the firewire cable was held straight in the z direction of the magnet bore. Fig. 1 shows photos of the experimental setup of the US system in the MRI scanners.

Two types of tracking were employed, namely passive tracking in the 3 T MRI system and active tracking in the 0.5 T MRI system. For passive tracking, four MR visible fiducial markers (Beekley MR-Spots, Bristol, CT) were attached to the US probe head to locate the US imaging direction. Fig. 1(b) shows the US probe with fiducial markers attached.

For active tracking in 0.5 T, an electromagnetic (EM) tracking system (EndoScout, Robin Medical, Baltimore, MD) was employed. A 9.4 mm × 9.4 mm × 9.4 mm EM tracker cube with a sensor coil on each face was fixed to the US probe head with a tailor-made plastic holder. The system measured the induced voltage on the sensor coils by MRI dynamic gradients (G_x , G_y , and G_z). Current from the gradient amplifiers into the gradient coils (I_x , I_y , and I_z) was also measured for reference. The system

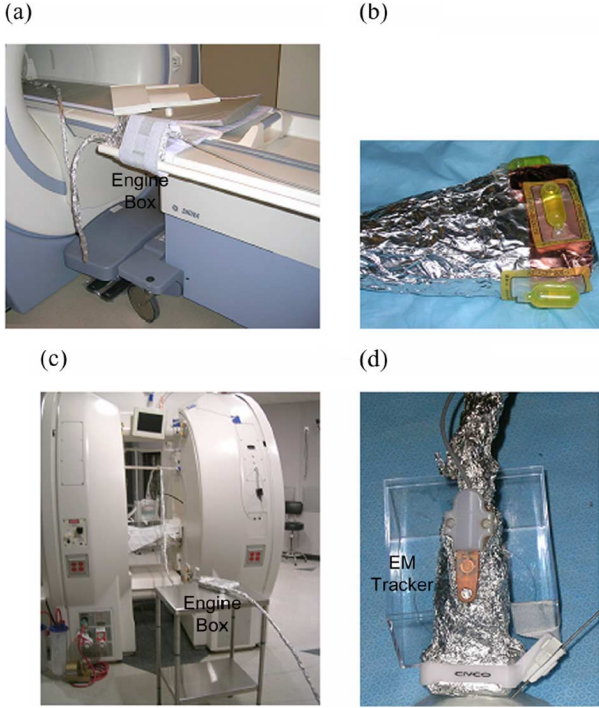


Fig. 1. Experimental setup of simultaneous MR/US imaging. (a) Shielded US in 3 T close bore MRI system, (b) US transducer head with MR visible fiducial markers attached, (c) shielded US in 0.5 T open bore MRI system and firewire cable routed orthogonal to the bore through the vertical gap, and (d) US transducer head with EM tracker and needle guide attached.

was then calibrated with the measurements and imaging data from fiducial targets of known distances to the tracker to establish a map of coordinate space. Sensor voltages, gradient coil currents, and the calibration map are essential for establishing the location and orientation of the tracker attached to any rigid instrument to be tracked [31]. The aluminum shielding was opened at the EM tracker in order not to attenuate the gradient signal. Fig. 1(d) shows the US probe with the tracker on top of the aluminum shielding and the MR compatible needle guide (Civco Medical Solutions, Kalona, IA).

B. Compatibility Test

To evaluate the interference between the two imaging systems and the effectiveness of aluminum shielding, baseline MR and US images were first captured with the unshielded US system placed outside the magnet room, and then repeated with the US transducer placed on the floor of the magnet room and at the isocenter of the bore. The test was then repeated where the US system was shielded and the aluminium shielding was grounded.

Compatibility was tested on both 0.5 T and 3 T MRI systems. In both cases, fast spin echo (FSE) sequences were selected. This is because FSE contains multiple high power 180° RF pulses that could lead to a worst case scenario of MRI interference effect on the US image quality. For experiments in the 3 T system, MR images of a loader phantom in a standard head coil were acquired. Acquisition parameters were as follows: FSE, TR= 800 ms, TE= 16.4 ms, receiver bandwidth= ± 31.25 kHz, ETL= 8, FOV= 300 mm, thick-

ness= 4 mm. The US imaging parameters were as follows: transmitting frequency= 7.5 MHz, DOV= 5 cm, 3 focuses, frame rate 16 fps. For 0.5 T, MR images of a CuSO_4 solution phantom were acquired, with the use of a pair of flexible linear butterfly coil with loops of size 20 cm \times 20 cm each. Acquisition parameters were as follows: FSE, TR= 616 ms, TE= 96 ms, receiver bandwidth= ± 31.25 kHz, ETL= 16, FOV= 370 mm. The US imaging parameters were as follow: transmitting frequency= 7.5 MHz, DOV= 5 cm, single focus= 2.8 cm, frame rate 64 fps.

To quantify the degree of interference of the US system on MR image quality, MRI noise-only images were collected. The images were acquired with the MRI system RF transmitter power turned off, so that spins of the phantom were not excited and no signal was emitted. Thus, the resulting image was a noise image pattern which included system noise and noise induced by electromagnetic interference. In addition, the US was tuned to different transmitting frequencies (5, 6, 7.5, 9 MHz) to visualize its effects on the noise pattern in MRI. MR images were captured twice for every scenario to visualize any changes in the image noise pattern over time. For comparison of the noise in MR images, the values of the MRI receiver gains were fixed and the MRI transmitter power was set to zero. The transmitter power was then restored to its original value for acquisition of phantom images.

To establish the effects of MRI on US, US images were acquired with the US probe placed at the isocenter and the MRI operating continuously for image acquisition. The quality of the US images with the probe window covered with a single layer of foil was compared to the case with no foil. An additional set of MRI parameters (FSE, TR= 600 ms, TE= 6.16 ms, receiver bandwidth= ± 31.25 kHz, ETL= 8, FOV= 300 mm) was applied to see the effects on the US image noise pattern due to changes in the MRI acquisition parameters.

The number of US frames corrupted with noise due to MRI interference was counted and the US frame rate was recorded. The artifact source pulse duration, P_d , and the separation between the artifact pulses, P_s , in the corrupted frame were calculated, by the given equations as follows:

$$P_d = \frac{P_w}{FW} \times \frac{1}{FR} \quad (1)$$

and

$$P_s = \frac{P_{sep}}{FW} \times \frac{1}{FR} \quad (2)$$

where

P_d = artifact pulse duration (ms)

P_s = artifact pulse separations (ms)

P_w = artifact pulse width (pixel)

P_{sep} = separation between artifact pulses (pixel)

FW = US frame width (pixel)

FR = US frame rate (fps).

P_w is measured at the full-width half-maximum (FWHM) of the artifact intensity.

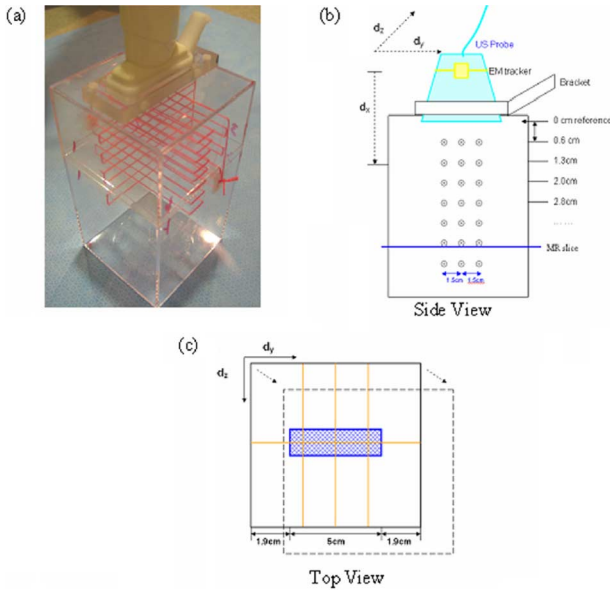


Fig. 2. Calibration phantom used for calibrating the active tracking system. (a) Photograph of the calibration phantom with MR/US visible strings and US probe attached. (b) Side view of the schematic diagram of the US calibration box. (c) Top view of the schematic diagram of the US calibration box. dx , dy , and dz are the three offsets to be specified.

C. Calibration for Active Tracking

As an alternative to retrospective image registration, active tracking was used to acquire the MR image in the same plane as the US image. A calibration step was necessary to establish correspondences. A calibration phantom with dual modality fiducials was created, using a rectangular plastic box filled with CuSO_4 solution. Grids of string were placed at depths corresponding to the focal depths available in the US system software (0.6, 1.3, 2.0, 2.8, 3.5, 4.5, 5.5, and 6.5 cm). The intersections of perpendicular segments of the string were treated as fiducials and were visible in both modalities. Intersections were at 0 cm (center) and ± 1.5 cm off center. A needle guide bracket that fit the US probe head was integrated into the top of the phantom to affix the US probe, such that the center of the US image contains the central string crossing and the lateral string intersections were also in the imaging plane.

To calibrate the position of the EM tracker with respect to the coordinate space inside the magnet bore, an US image orthogonal to the MR images was simultaneously acquired. An EM tracking parameter file describing the geometry offsets was built. It is necessary to calibrate the EM tracking only once for each tool, if the distance and orientation between the tracker cube and the tracked tool remain unchanged. In this study, the tracked tool is the imaging face of the US probe. Fig. 2 shows the calibration phantom and the offset parameters that ought to be specified in the parameter file.

Coronal MR images were captured continuously with location increment in the x direction (along dx in Fig. 2) until the string crossings entered the coronal scan plane. The offset errors between the MR image center and central string crossing (dy and dz) were measured. These dx , dy , and dz parameters

were used to update the EM tracker parameter file. Two iterations were performed converge on the solution for this calibration process. The calibration was then validated by acquiring a MR image coplanar to the US image and noting the location of the string intersections. Note that the EM tracker parameter file did not have a provision to correct for angular error.

D. Clinical Applications—Needle Guided Breast Biopsy

To demonstrate the feasibility for fast target definition for biopsy needle puncture, a fiducial target in a 10% Polyvinyl Alcohol cryo-gel (PVA-C) breast phantom was localized by free hand US in the magnet bore. PVA-C was chosen for molding the phantom because it has similar acoustic, T1 and T2 properties as human tissue, such that it is visible in both US and MRI [32].

For the 0.5 T system, MRI scans were acquired using a 20 cm \times 20 cm single loop flexible surface coil. To perform biopsy, the US needle guide was attached to the US probe head to position the MR-compatible needle along the desired trajectory. Two-dimensional FSE MR images were acquired for the whole volume prior to biopsy. US (30 fps) and MRI scans were then simultaneously acquired at the same imaging plane while the biopsy needle was advanced to the target. For the MRI, a single slice MR image was captured continuously at the same imaging plane, and the time required to capture a slice is 16 s. Thus, the “refresh rate” of an MRI scan was 16 s. MRI parameters were: FSE, TR/TE = 1000/96 ms, ETL = 16, slice thickness = 5 mm, FOV = 256 mm \times 256 mm. MR images were sent directly to a real-time workstation (GE Healthcare, Milwaukee, WI), already interfaced with the scanner to enable scan plane control.

For biopsy in the 3 T system, a MR localizer scan was first acquired to locate the four fiducial markers attached to the US probe head that indicated the probe location and imaging orientation. An oblique MR scan plane was then established manually according to the positions of the markers. Thus, the cutting plane of all subsequent MR scans could coincide with that of US. A biopsy needle was then advanced to the fiducial target during dynamic MRI and real time US. No calibration was needed between MRI and US.

III. RESULTS

A. Compatibility Test

Two types of noise, namely broadband noise and narrowband “zippers” were observed on the MR images when the US system was introduced into the magnet room. The MRI signal degraded significantly and no image could be seen when the US probe was placed at the isocenter without any shielding. However, with proper RF shielding of the cables and US probe, interference from US operation to MRI was greatly reduced. Fig. 3 shows the comparison of MR image noise under different experimental setups at different magnetic field strength, with MRI RF transmitter power turned off.

To measure the rise in the broadband noise, which is the background image noise, the mean and standard deviation were measured, by choosing regions of interest (ROI) in each of the MR image while the regions with periodic zippers were excluded.

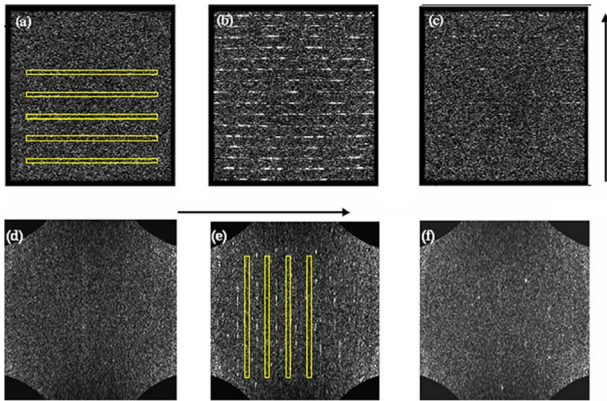


Fig. 3. Comparison of MR image noise at 3 T (upper row) and 0.5 T (lower row) under various conditions of US setup with MR RF transmitter powered off, [(a), (d)] baseline image without US, [(b), (e)] during US capturing with US system shielded and probe window unshielded, [(c), (f)] during US capturing with shielded US system and shielded probe window. The arrows indicate the direction of frequency encoding. Rectangles indicate the ROI drawn for noise measurements.

TABLE I
IMAGE NOISE MEASUREMENT OF MRI IN 0.5 T AND 3 T

Measurement conditions		Baseline, without US	US probe at isocenter, without shielding	US probe at isocenter, shielded, probe window open	US probe at isocenter, shielded, probe window with single layer of foil
0.5 T	Background noise ROI mean (s.d.)	8.98(4.78)	NIL	10.87 (6.50)	9.48 (5.05)
	Observations Mean(s.d.)	Image is clean	Coil detune, no signal measured	Increase 21.01% (35.98%)	Increase 5.57% (5.65%)
3T	Background noise ROI mean (s.d.)	4.61(2.66)	NIL	5.23(3.34)	4.83(2.84)
	Observations Mean(s.d.)	Image is clean	Coil detune, no signal measured	Increase 13.55% (25.5%)	Increase 4.87% (6.87%)

The ROI was shown in Fig. 3(a) and (e). For fair measurement and comparison, the same set of ROI was applied to all the MR images acquired under the same field strength. The MRI broadband noise measurements based on the defined ROIs are shown in Table I.

The broadband noise increased by around 21.01% in 0.5 T and 13.55% in 3 T compared to the baseline image when the US probe window was open. However, with proper shielding of the probe window, the increase in noise intensity dropped to 5.57% in 0.5 T and 4.87% in 3 T, respectively, compared to the baseline with no US placed. This 5%–6% increase in background noise was negligible when the RF was turned on since signals from the phantom were dominant.

Narrowband periodic zippers, as shown in Fig. 3(b) and (d), were clearly observed when the US probe window was open while the rest of the US system was shielded. Fig. 3(c) and (f) show that when the US probe window was covered with a single layer of aluminum foil, the zippers were greatly reduced. The zippers were seen along the frequency encoding directions (i.e., zippers lines were perpendicular to the frequency encoding axis). There was no drift of the zipper locations over time when the MRI and US acquisition parameters remained unchanged. However, the intensity of the bright spots in the zippers was

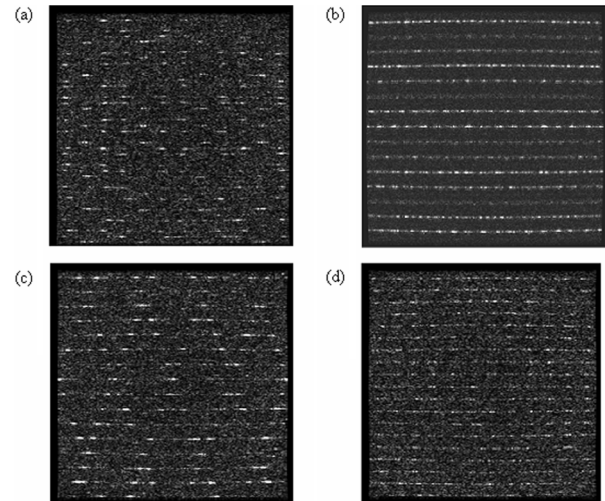


Fig. 4. 3 T MRI zipper noise pattern with different US transmitting frequencies. (a) 5 MHz, (b) 6 MHz, (c) 7.5 MHz, and (d) 9 MHz.

different over time. Zipper separations decreased when the US transmitting frequencies increased. Fig. 4 shows the change in zipper noise pattern in 3 T MRI when the US transmitting frequencies was altered while all other US imaging parameters were stayed identical.

For artifacts in US, vertical strips were observed on some US frames intermittently during MRI imaging. The effect of the MRI RF transmission pulses on US images was negligible when the probe head window was covered with a single layer of foil.

Fig. 5 shows the interference in US images due to the 3 T MRI system with different MRI parameters. Interference was observed near the bottom of the US image. For the case with TR= 800 ms, the separation between corrupted frames was about 800–900 ms. The artifact source pulse duration, P_d , had a duration of around 0.9–1.0 ms. The separations between pulses, P_s , were about 8.0–8.2 ms. For the case with TR= 600 ms, the separation between corrupted frames was about 600 ms. The artifact course pulse duration, P_d , had duration of around 0.9–1.1 ms, while the separations between pulses, P_s , were about 11.6–12.1 ms.

For the results in the 0.5 T MRI system, similar artifact characteristics were observed. A corrupted US frame was observed for every 35–40 US frames captured intermittently, while the US frame rate was 64 fps. Thus, the separations between corrupted frames were about 550–625 ms.

B. Needle Guided Breast Biopsy

The calibration accuracy for establishing offset parameters in the EM tracking parameter file was illustrated in Fig. 6. The US image shows the string crossings of the calibration phantom at fixed focal depths. The cross-hairs in the MRI images indicate the center of the image before and after the calibration iterations. The offset errors (dy and dz) were corrected after the iterations.

Fig. 7 shows the simultaneous MR/US scan of the 10% PVA-C breast phantom with a glass bead or a fiducial marker as the target in 0.5 T and 3 T, respectively. Fig. 7(c) shows the volume rendered MRI images with 2-D US frame. The fiducial markers used for passive tracking were shown. Biopsy needle

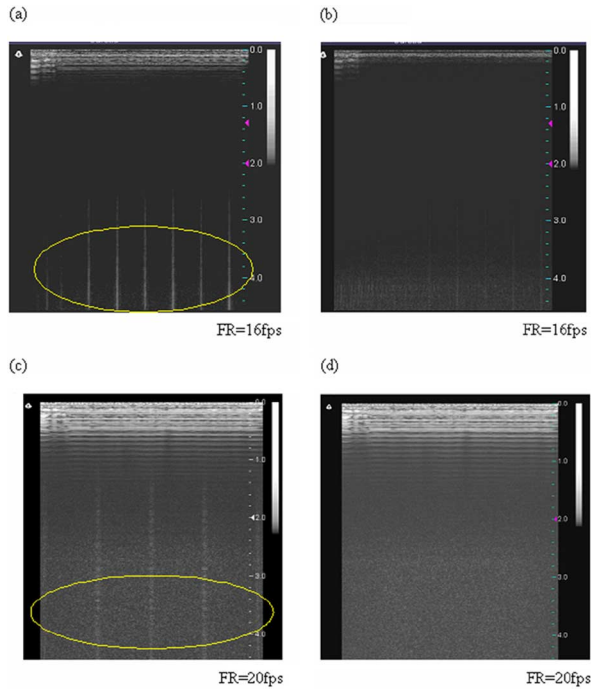


Fig. 5. US images with probe at isocenter of 3 T MRI system while MRI is running with [(a), (b)] TR= 800 ms, and [(c), (d)] TR= 600 ms. (a), (c) With US probe window unshielded. (b), (d) US probe window shielded with a single layer of foil. Yellow ellipse indicates the vertical strips at the bottom.

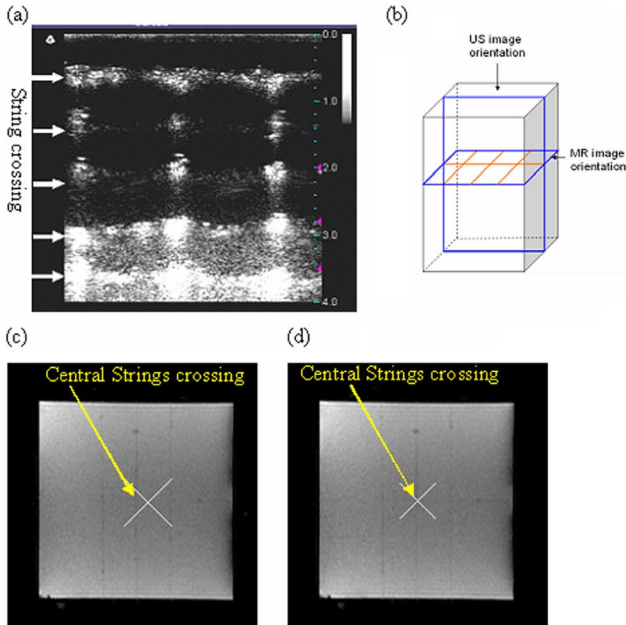


Fig. 6. US and MR images captured during active tracking calibration in 0.5 T. (a) US image of calibration phantom showing string crossings. (b) A representation of strings and location of MR and US images. (c) MR image corresponding to US focal depth of 4.5 cm at the first iteration of calibration and (d) after final iteration of calibration.

was inserted and advanced through the needle guide grid lines displayed on the US software interface. MRI and US images were captured simultaneously in the same scan plane location and orientation.

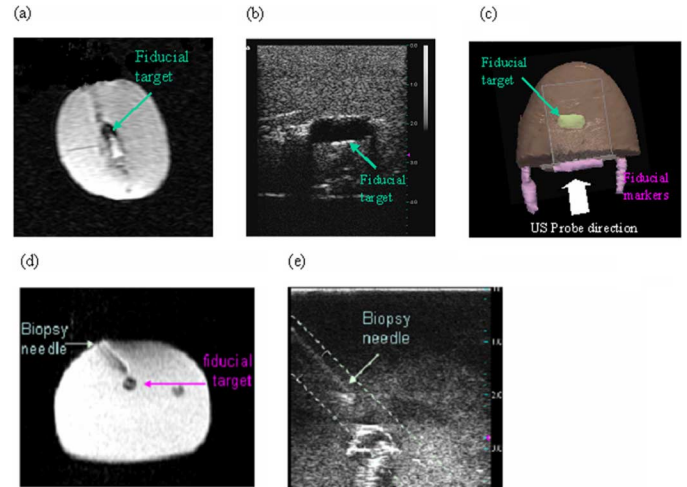


Fig. 7. Simultaneous MR/US images of biopsy needle targeting. (a) MRI breast image with fiducial target in 3 T, (b) US image of the fiducial target with US in 3 T MRI system, (c) 2-D US image fused with a rendered MRI volume, with passive fiducial markers tracking in 3 T (d) MRI breast image in 0.5 T and (e) the corresponding US image with real time active tracking in 0.5 T.

IV. DISCUSSION

The compatibility test suggested that US and MRI could operate together provided we can minimize the interference. The broadband noise in MRI originated from digital switching in the US beam-former engine box and the switching in the firewire during digital signal transmission. No broadband noise was observed when the firewire and the digital switching of the engine box was inactive, even when the US probe was placed in the isocenter of the magnet bore without any shielding. With the introduction of aluminum foils as the RF shielding along the entire US probe and the firewire cable, broadband noise was much reduced. Aluminum foil, therefore, could serve as a temporary shielding for the US system as confirmed by our experiments.

Periodic zippers noise was originated from the short high-voltage pulses applied to the piezo-electric crystal. Altering the US transmitting frequency changed the pattern of the zippers. The zipper separations decreased with the increase in US transmitting frequencies. The zippers lines were always perpendicular to the frequency encoding axis, indicating that the short high-voltage pulses caused interference in specific narrow frequency ranges in MRI during its acquisitions. This created zipper-like pattern in the MRI images. Covering the probe window with a single layer of aluminum foil reduced the zippers effectively.

Vertical strip noise in US images was likely due to the RF pulses of the MRI system. The vertical strips pulse duration, P_d , was about 0.9–1.1 ms in the 3 T tests. The repetitive strip pulse separation, P_s , was about 8.0 ms and 12.0 ms, respectively, in the 3 T tests with different FSE settings. The P_d was too wide (about 1 ms wide in all cases), making it unlikely that it was caused by the imaging gradient ramps. The repetitive nature of the strips with constant intensity and depth, separated by constant time (several milliseconds), showed a very plausible explanation that that the artifact was possibly originated from the 180° MRI RF pulses. The occurrence of corrupted US frames tended to be correlated with the TR of the MRI. The corrupted

US frames occurred every 800–900 ms and 600 ms in the compatibility test in 3 T, where the TR was 800 ms and 600 ms, respectively. The occurrence of US frames in 0.5 T test was around 600 ms where the corresponding MRI sequence had a TR of 616 ms. Since the interference was possibly due to the MRI RF pulses, changing the TR may change the frequency of occurrences of the corrupted frames, while changing the TE and ETL may affect the separation of pulses, P_s , within the corrupted frame.

This interference in US was negligible when the probe head window was covered with a single layer of foil, but that caused some signal degradation in the US images. The signal degradation was remedied by tuning up the time gain compensation (TGC) amplification in the US system. TGC adjusts and balances the US image by equalizing the brightness of echoes from near field to far field. By increasing the overall TGC, the internal structures could still be seen clearly in the presence of one layer of foil. Nevertheless, the corrupted frames may be discarded by active blanking of the US through firing triggering pulses from MRI during RF pulsing or by retrospective blanking of the corrupted US frames.

In simultaneous MR/US guided biopsy, the high temporal resolution of US allows a fast feedback of the current needle tip position during the biopsy process. In our 3 T test, US had a frame rate of 30 fps while MRI had an acquisition time of 16 seconds per slice. With the introduction of US, one does not need to wait for the MR image to refresh before advancing the needle. Thus US can be used to place the biopsy needle in real time inside the magnet bore, while MRI could be relegated to the role of confirming the trajectory and final needle location.

EM tracking is a convenient tool for tracing the positions of US probe inside the magnet bore. Unlike optical tracking, which identifies the co-ordinate of the tracked tool by using a camera to locate the LEDs or reflective spheres mounted on the tools with a camera [16], [33], the EM trackers do not need to be within the line of sight of any camera. In EM tracking, only a simple calibration step is required to modify the tool file in matching the coordinates of the trackers to the coordinates of the image plane. Once the calibration is completed, the MRI imaging plane could automatically follow the coordinate of the EM tracker.

Passive tracking by attaching MRI visible markers to the US probe is an inexpensive and simple method in tracking the US imaging plane. No calibration is needed. This method could be applied to close bore MRI systems with limited space or MRI sites limited resources. However, one major disadvantage of passive tracking is that the accuracy of the MRI scan plane prescription is limited by the ability to localize the markers. Nevertheless, this method could still be implemented in situations requiring only the rough location of tools inside the magnet bore and where other types of tracking systems are not available. Moreover, postprocessing steps could be performed to register the US and MRI images to compensate for the error.

A limitation of our study was that only an FSE MRI pulse sequence was employed to assess compatibility. The US induced artifacts may appear more intense in MR images acquired with pulse sequences inherently low in signal-to-noise ratio. Moreover, sequences utilizing a high acquisition bandwidth such as echo planar imaging and steady state free precession will ex-

hibit zippers that are apparently compressed (more narrow) but greater in number across the images. Further studies may be needed.

Some other limitations of the experimental setup were also noted. The aluminum foil was paramagnetic and was slightly attracted to the magnet bore. Electric charges accumulated easily on the foil with time, even when the foil was grounded, giving rise to the broadband noise in MRI. Cutting the aluminum foils into strips reduced the accumulation of charges and avoided the rise in broadband noise. Also, the aluminium foil cracked easily. In future, it is better to replace the aluminium foil with other permanent shielding such as copper braid mesh tubes.

A small signal degradation was observed in part of the MRI image, at the surface of the breast phantom in contact with where the US transducer head. This artifact was due to the presence of nonferromagnetic metallic objects inside the US transducer head and exacerbated by eddy currents in the aluminum foil. This problem can be solved by adding a water balloon or other US transmission materials with a low US attenuation coefficient, as an acoustic coupling layer between the US probe head and the object being imaged. The layer keeps the transducer head away from the object surface but with a low attenuation coefficient that allows acoustic waves to pass through with insignificant signal attenuation.

Finally, guidance accuracy of the biopsy needle insertion using the proposed MR/US imaging system has not been statistically addressed in our study. Biopsy success could be quantified with the use of a tissue mimic phantom with a fiducial target of a color and material different from the surrounding phantom [17], [20]. The guidance process would be counted as success if the biopsy sample contained the material comprising the fiducial target. The experiment could be repeated with MRI-guidance alone for comparison of success rate with the hybrid MR/US system.

V. CONCLUSION

In this work, we have discussed in detail the compatibility issues and the practical setup of simultaneous MR/US imaging. We have also demonstrated in phantom one possible application: breast biopsy. One extension of our work is to quantify the guidance errors as discussed. Another possible direction is to apply active tracking in high field close bore magnet. Our method of simultaneous MR/US imaging for needle guidance can also be extended to other parts of the body and potentially help in other guided therapies such as RF ablation and cryotherapy for minimally invasive surgery [34].

ACKNOWLEDGMENT

The authors would like to thank S. Dimaio, E. Samset, M. Brodsky, and M. Ottensmeyer for their technical help in phantom molding, system development, and machining the attachment piece between the EM probe and US transducer.

REFERENCES

- [1] A. Ganguly, Z. Wen, B. L. Daniel, K. Butts, S. T. Kee, V. Rieke, H. M. Do, N. J. Pelc, and R. Fahrig, "Truly hybrid X-ray/MR imaging: Toward a streamlined clinical system," *Acad. Radiol.*, vol. 12, pp. 1167–77, Sep. 2005.

- [2] H. Yu, R. Fahrig, and N. J. Pelc, "Co-registration of x-ray and MR fields of view in a hybrid XMR system," *J. Magn. Reson. Imag.*, vol. 22, pp. 291–301, Aug. 2005.
- [3] K. S. Rhode, M. Sermesant, D. Brogan, S. Hegde, J. Hipwell, P. Lambiase, E. Rosenthal, C. Bucknall, S. A. Qureshi, J. S. Gill, R. Razavi, and D. L. Hill, "A system for real-time XMR guided cardiovascular intervention," *IEEE Trans. Med. Imag.*, vol. 24, no. 11, pp. 1428–40, Nov. 2005.
- [4] T. Beyer, D. W. Townsend, T. Brun, P. E. Kinahan, M. Charron, R. Roddy, J. Jerin, J. Young, L. Byars, and R. Nutt, "A combined PET/CT scanner for clinical oncology," *J. Nucl. Med.*, vol. 41, pp. 1369–79, Aug. 2000.
- [5] T. F. Hany, H. C. Steinert, G. W. Goerres, A. Buck, and G. K. von Schulthess, "PET diagnostic accuracy: Improvement with in-line PET-CT system: Initial results," *Radiology*, vol. 225, pp. 575–81, Nov. 2002.
- [6] M. M. Maher, M. K. Kalra, A. Singh, M. A. Blake, S. L. Aquino, A. J. Fischman, and P. R. Mueller, "Hot" spots in hybrid positron emission tomography/computed tomography scanning of the abdomen: Protocols, indications, interpretation, responsibilities, and reimbursements," *Curr. Probl. Diagn. Radiol.*, vol. 35, pp. 35–54, Mar.–Apr. 2006.
- [7] P. K. Marsden, D. Strul, S. F. Keevil, S. C. Williams, and D. Cash, "Simultaneous PET and NMR," *Br. J. Radiol.*, vol. 75, pp. S53–9, Nov. 2002.
- [8] M. D. Seemann, "Whole-body PET/MRI: The future in oncological imaging," *Technol. Cancer Res. Treat.*, vol. 4, pp. 577–82, Oct. 2005.
- [9] L. A. Crowe, B. Ariff, J. Keegan, R. H. Mohiaddin, G. Z. Yang, A. D. Hughes, S. A. McG Thom, and D. N. Firmin, "Comparison between three-dimensional volume-selective turbo spin-echo imaging and two-dimensional ultrasound for assessing carotid artery structure and function," *J. Magn. Reson. Imag.*, vol. 21, pp. 282–9, Mar. 2005.
- [10] P. J. Slomka, J. Mandel, D. Downey, and A. Fenster, "Evaluation of voxel-based registration of 3-D power Doppler ultrasound and 3-D magnetic resonance angiographic images of carotid arteries," *Ultrasound Med. Biol.*, vol. 27, pp. 945–55, Jul. 2001.
- [11] A. J. Martin, L. K. Ryan, A. I. Gotlieb, R. M. Henkelman, and F. S. Foster, "Arterial imaging: Comparison of high-resolution US and MR imaging with histologic correlation," *Radiographics*, vol. 17, pp. 189–202, Jan.–Feb. 1997.
- [12] F. P. Glor, B. Ariff, A. D. Hughes, L. A. Crowe, P. R. Verdonck, D. C. Barratt, S. A. McG Thom, D. N. Firmin, and X. Y. Xu, "Image-based carotid flow reconstruction: A comparison between MRI and ultrasound," *Physiol. Meas.*, vol. 25, pp. 1495–509, Dec. 2004.
- [13] M. M. Letteboer, P. W. Willems, M. A. Viergever, and W. J. Niessen, "Brain shift estimation in image-guided neurosurgery using 3-D ultrasound," *IEEE Trans. Biomed. Eng.*, vol. 52, no. 2, pp. 268–76, Feb. 2005.
- [14] N. Hata, T. Dohi, H. Iseki, and K. Takakura, "Development of a frameless and armless stereotactic neuronavigation system with ultrasonographic registration," *Neurosurgery*, vol. 41, pp. 608–13, Sep. 1997.
- [15] D. G. Gobbi, R. M. Comeau, B. K. H. Lee, and T. M. Peters, "Integration of Intra-operative 3-D Ultrasound with pre-operative MRI for neurosurgical guidance," presented at the 22th Annu. EMBS Int. Conf., Chicago, IL, 2000.
- [16] F. Lindseth, J. H. Kaspersen, S. Ommedal, T. Lango, J. Bang, J. Hokland, G. Unsgaard, and T. A. Hernes, "Multimodal image fusion in ultrasound-based neuronavigation: Improving overview and interpretation by integrating preoperative MRI with intraoperative 3 D ultrasound," *Comput. Aided Surg.*, vol. 8, pp. 49–69, 2003.
- [17] C. A. Piron, P. Causer, R. Jong, R. Shumak, and D. B. Plewes, "A hybrid breast biopsy system combining ultrasound and MRI," *IEEE Trans. Med. Imag.*, vol. 22, no. 9, pp. 1100–1110, Sep. 2003.
- [18] J. M. Blackall, G. P. Penney, A. P. King, and D. J. Hawkes, "Alignment of sparse freehand 3-D ultrasound with preoperative images of the liver using models of respiratory motion and deformation," *IEEE Trans. Med. Imag.*, vol. 24, no. 11, pp. 1405–1416, Nov. 2005.
- [19] H. M. Verkooijen, "Diagnostic accuracy of stereotactic large-core needle biopsy for nonpalpable breast disease: Results of a multicenter prospective study with 95% surgical confirmation," *Int. J. Cancer*, vol. 99, pp. 853–9, Jun. 20, 2002.
- [20] W. L. Smith, K. J. Surry, A. Kumar, L. McCurdy, D. B. Downey, and A. Fenster, "Comparison of core needle breast biopsy techniques: Freehand versus three-dimensional US guidance," *Acad. Radiol.*, vol. 9, pp. 541–50, May 2002.
- [21] K. J. Surry, W. L. Smith, L. J. Campbell, G. R. Mills, D. B. Downey, and A. Fenster, "The development and evaluation of a three-dimensional ultrasound-guided breast biopsy apparatus," *Med. Image Anal.*, vol. 6, pp. 301–312, Sep. 2002, 2002.
- [22] M. Van Goethem, W. Tjalma, K. Schelfout, I. Verslegers, I. Biltjes, and P. Parizel, "Magnetic resonance imaging in breast cancer," *Eur. J. Surg. Oncol.*, vol. 32, pp. 901–10, Nov. 2006.
- [23] S. G. Orel and M. D. Schnall, "MR imaging of the breast for the detection, diagnosis, and staging of breast cancer," *Radiology*, vol. 220, pp. 13–30, Jul. 2001.
- [24] B. L. Daniel, R. L. Birdwell, K. Butts, K. W. Nowels, D. M. Ikeda, S. G. Heiss, C. R. Cooper, S. S. Jeffrey, F. M. Dirbas, and R. J. Herfkens, "Freehand iMRI-guided large-gauge core needle biopsy: A new minimally invasive technique for diagnosis of enhancing breast lesions," *J. Magn. Reson. Imag.*, vol. 13, pp. 896–902, Jun. 2001.
- [25] S. G. Silverman, B. D. Collick, M. R. Figueira, R. Khorasani, D. F. Adams, R. W. Newman, G. P. Topulos, and F. A. Jolesz, "Interactive MR-guided biopsy in an open-configuration MR imaging system," *Radiology*, vol. 197, pp. 175–81, Oct. 1995.
- [26] A. M. Tang, D. F. Kacher, E. Y. Lam, M. Brodsky, F. A. Jolesz, and E. S. Yang, "Multi-modal Imaging: Simultaneous MRI and ultrasound imaging for carotid arteries visualization," presented at the 29th Annu. Conf. IEEE Eng. Med. Biol. Soc., Lyon, France, 2007.
- [27] A. M. Tang, D. F. Kacher, K. K. Wong, G. Li, F. A. Jolesz, and E. S. Yang, "MRI-comptaible ultrasound for image guided therapy," in *Proc. 14th Scientific Meeting ISMRM*, Seattle, 2006, p. 1414.
- [28] M. Gunther and D. A. Feinberg, "Ultrasound-guided MRI: Preliminary results using a motion phantom," *Magn. Reson. Med.*, vol. 52, pp. 27–32, Jul. 2004.
- [29] R. Chopra, L. Curiel, and K. Hynynen, "Progress in multimodality imaging: Truly simultaneous ultrasound and magnetic resonance imaging," in *Proc. 15th Scientific Meeting, ISMRM*, Berlin, Germany, 2007, pp. 295–295.
- [30] P. Risholm and E. Samset, "Registration free us-mr fusion for identification of infravicular parts of plexus brachialis," presented at the 20th Int. Congress Computer Assisted Radiol. Surgery, Osaka, Japan, 2006.
- [31] D. F. Kacher, S. P. DiMaio, E. Samset, B. Fetics, E. Nevo, and F. A. Jolesz, "Towards MRI-guided vascular intervention with an electromagnetic tracking system and 3-D navigation software," in *14th Sci. Meeting, Int. Soc. Mag. Reson. Med.*, Seattle, WA, 2006.
- [32] K. J. Surry, H. J. Austin, A. Fenster, and T. M. Peters, "Poly(vinyl alcohol) cryogel phantoms for use in ultrasound and MR imaging," *Phys. Med. Biol.*, vol. 49, pp. 5529–5546, Dec. 21, 2004, 2004.
- [33] The NDI Polaris System [Online]. Available: <http://www.ndigital.com/polaris.php> Jun. 2006
- [34] D. F. Kacher and F. A. Jolesz, "MR imaging-guided breast ablative therapy," *Radiol. Clin. North Amer.*, vol. 42, pp. 947–962, Sep. 2004, vii.